

Article

Improving Effect of Graphene on Electrochemical Properties of Fe₂O₃ Anode Materials

Guanglin Zhu, Bo Gao , Ganfeng Tu, Haifeng Liu and Ming Wang

Key Laboratory for Ecological Metallurgy of Multimetallurgical Mineral (Ministry of Education), Northeastern University, Shenyang 110819, China; zhuguanglin@stumail.neu.edu.cn (G.Z.); tugf@smm.neu.edu.cn (G.T.); liuhaifeng@stumail.neu.edu.cn (H.L.); wangming@stumail.neu.edu.cn (M.W.)
* Correspondence: gaob@smm.neu.edu.cn

Abstract: Transition metal oxides have a high initial charge-discharge capacity of 800–1000 mAh/g, the electrochemical performance, cyclic performance and rate performance of the composite of transition metal oxide and graphene have been improved due to the unique two-dimensional structure and excellent electrical conductivity of graphene. In this paper, iron oxides materials with different morphs were prepared by different hydrothermal reaction temperatures, and rGO/Fe₂O₃-175 °C composites with different graphene ratios were synthesized and used in the anode of lithium ion batteries. The results show that nanorod-shaped Fe₂O₃ had better electrochemical performance than spherical Fe₂O₃. 0.2rGO/Fe₂O₃-175 °C had the best cyclic performance, the first cyclic discharge capacity reaches 1372 mAh/g under the current density of 100 mA/g, and the cyclic reversible capacity remained at about 435 mAh/g after 50 cycles, illustrating that nanorods Fe₂O₃ and graphene composites can greatly buffer the volume expansion of Fe₂O₃.

Keywords: iron oxides; graphene; anode; lithium ion batteries; electrochemical performance



Citation: Zhu, G.; Gao, B.; Tu, G.; Liu, H.; Wang, M. Improving Effect of Graphene on Electrochemical Properties of Fe₂O₃ Anode Materials. *Metals* **2022**, *12*, 593. <https://doi.org/10.3390/met12040593>

Academic Editor: Yoshikazu Ito

Received: 2 March 2022

Accepted: 28 March 2022

Published: 30 March 2022

Publisher's Note: MDPI stays neutral with regard to jurisdictional claims in published maps and institutional affiliations.



Copyright: © 2022 by the authors. Licensee MDPI, Basel, Switzerland. This article is an open access article distributed under the terms and conditions of the Creative Commons Attribution (CC BY) license (<https://creativecommons.org/licenses/by/4.0/>).

1. Introduction

Transition metal oxides have high cyclic stability and theoretical specific capacity, and their initial charge-discharge capacity is 800–1000 mAh/g, approximately 2–3 times higher than that of carbon materials [1–4]. Compared with other transition metal oxides, iron oxides have the advantages of low raw material price, easy preparation, stable chemical properties and high theoretical specific capacity. Therefore, iron oxides as anode materials for lithium ion batteries have high research value. However, iron oxides have the problems of volume change and poor conductivity in the charging and discharging process, which leads to poor cycling performance and seriously hinders its engineering application [5–9]. The advantages of combining transition metal oxides and carbon materials are a more stable structure and an excellent electron transport channel between the current collector and the active substance, which is helpful for the avoidance of SEI film formation [10–12]. The carbon-coated α -Fe₂O₃ nano-structure on stainless steel substrates prepared through simple pyrolytic deposition of ferrocene is used as anode materials for lithium ion batteries, this anode material can still possess a high reversible capacity of 1138 mAh/g after 300 cycles at a current density of 500 mA/g, and it can also sustain a capacity of 458.8 mAh/g after the cycle even at a high current density of 10,000 mA/g [13].

Due to the high theoretical specific surface area, unique two-dimensional structure, excellent thermal and electrical conductivity of graphene, the electrochemical performance, cyclic performance and rate performance of the composite of transition metal oxide and graphene have been improved [14–17]. Yang et al. [18] described a method for the fabrication of graphene-encapsulated metal oxides (GE-MO) through co-assembly between GO (Graphene Oxide) with a negative charge and oxide nanoparticles with a positive charge. The synthetic process is driven by the electrostatic interaction of the two substances, resulting in GE-MO by chemical reduction. The results indicated that GO-Co₃O₄ showed a

high reversible capacity of 1100 mAh/g in the first 10 cycles, and the reversible capacity still reached 1000 mAh/g after 130 cycles, showing excellent cycling performance. Therefore, it has great potential as an anode material for lithium storage. Lian et al. [19] developed a gas-liquid interface synthesis method to prepare nano-SnO₂/graphene composites, SnO₂ nanoparticles about 2–6 nm in size were uniformly distributed on the graphene matrix, they showed a high reversible specific capacity of 1304 mAh/g at 100 mA/g current density, and it still had a reversible capacity of 748 mAh/g even when the current density was increased to 1000 mA/g. The nano TiO₂/nitrogen doped graphene composites were synthesized by Cai et al. [20] through a gas/liquid interface reaction, and nitrogen atoms were successfully doped into graphene tablets, TiO₂ nanoparticles 8–13 nm in size were uniformly deposited on nitrogen doped graphene sheets. Compared with TiO₂/graphene composites and exposed TiO₂ nanoparticles, the nano TiO₂/nitrogen-doped graphene composites have better electrochemical properties, and still show a high capacity of 136 mAh/g at a current density of 1000 mA/g after 80 cycles.

Iron oxides were used to improve electrochemical performance by combining with graphene in a great deal of research. Zhou et al. [15] prepared Fe₂O₃/graphene nano-sheets by a simple and effective spray drying method, it sustained a capacity of 711 mAh/g after 50 times of charge and discharge, indicating improved cycle stability and rate performance. Fe₂O₃/graphene nanocomposites were also synthesized by Kan et al. [21] through the solvent hydrothermal method. In their study, Fe₂O₃ is grown on graphene and dispersed evenly to form a unique nano-sheet structure. Fe₂O₃/graphene obtained a high reversible capacity of 662.4 mAh/g after 100 cycles at 1000 mA/g. The significantly improved cycling performance is attributed to the unique structural affinity between Fe₂O₃ nano-sheets and graphene nano-sheets. Meng et al. [22] found that a-Fe₂O₃@graphene aerogel (a-Fe₂O₃@GA) composites used as anode materials for lithium ion batteries maintained a high reversible capacity of 745 mAh/g at a current density of 100 mA/g, and exhibited superior stable electrochemical cycling performance and excellent rate capability. In the above studies, the morphology of iron oxide is mainly spherical, there are few related studies on other morphology of iron oxide and graphene composites.

In this paper, nano-Fe₂O₃ was prepared at 220 °C, 205 °C, 190 °C and 175 °C, respectively. Fe₂O₃/graphene composites were synthesized by the PVP solvent assisted hydrothermal method. The phase composition and morphology were investigated by X-ray diffraction (XRD, Bruker-D8, Karlsruhe, Germany) and scanning electron microscopy (SEM, SSX-550, Shimadzu Corporation, Kyoto, Japan), and electrochemical properties were tested by constant current charge-discharge, cyclic voltammetry and AC impedance.

2. Experimental

2.1. Anode Material Preparation

The reagents in the paper were purchased from Sinopharm Chemical Reagent Co., Ltd. (Shenyang, China), which were of analytical grade (AR).

Preparation of nano ferric oxide: Firstly, 16 g FeCl₃·6H₂O was dissolved in 300 mL deionized water. During the stirring process, sodium hydroxide solution was dropped at the same time until the pH of the solution reached 10. Then, the solution was loaded into a high-pressure reactor (Sinopharm Chemical Reagent Co., Ltd., Shenyang, China) and reacted at different hydrothermal temperatures (220 °C, 205 °C, 190 °C, 175 °C) for 12 h. After cooling and centrifuge separation, the final product Fe₂O₃ was obtained by drying at 60 °C for 12 h and calcination at 300 °C for 3 h.

Preparation of GO (modified Hummers method): the appropriate amount of graphite and potassium permanganate was mixed evenly, and slowly added into the mixture of H₂SO₄ and H₃PO₄. After stirring at 50 °C for 12 h, the gray-green solution was poured into ice cubes for cooling, then H₂O₂ was slowly added, the solution turned bright yellow and stirred for 30 min, and graphite oxide was obtained after washing and drying.

Preparation of reduced graphene/iron oxide composite (rGO/Fe₂O₃): Appropriate amount of GO was dispersed in deionized water by ultrasound for 1 h to obtain GO

dispersed suspension. A certain mass of Fe_2O_3 and 0.45 g polyvinylpyrrolidone (PVP) were, respectively, dissolved in GO dispersion (where the mass ratio of Fe_2O_3 to GO was 1:0, 1:0.1, 1:0.2, 1:0.3, 1:0.4, 1:0.5). After 30 min ultrasound, the samples were transferred to the high-pressure reactor, followed by hydrothermal reaction at 175 °C for 12 h, centrifugation and drying for 12 h, and Ar calcination at 300 °C for 3 h to obtain different ratios of rGO/ Fe_2O_3 .

2.2. Preparation of Electrode Sheet

According to the active substance: acetylene black: PVDF (polyvinylidene fluoride) = 8:1:1 mass ratio to weight, first of all, the binder PVDF and n-methyl-2-pyrrolidone organic solvent was mixed and stirred, and then mixed with other substances into a uniform slurry. Then the paste was evenly coated on copper foil and put into a vacuum drying oven (BZF-50, Shanghai Boxun Industrial Co., Shanghai, China) to dry. Finally, the sheet was washed and pressed to obtain the electrode sheet.

2.3. Assembly of Lithium Ion Button Battery

The electrode sheet was placed in a glove box filled with argon to assemble the CR2032 button battery. The mixture of 1 mol·L⁻¹ LiPF₆/ethylene carbonate (EC) + dimethyl carbonate (DMC) (volume ratio: 1:1) was used as the electrolyte, and the electrode was assembled in the sequence of negative shell → spring sheet → lithium sheet gasket → diaphragm → electrode sheet → positive shell. The assembled semi-battery was sealed in time, and the open-circuit voltage was detected to determine whether it was normal. The electrochemical performance was tested after standing for 12 h.

The lithium sheet, copper foil, gasket and spring sheet involved in the battery preparation process were purchased from Shanghai Shunyou Metal Materials Co., Ltd. (Shanghai, China), and the polypropylene microporous film was produced from Celgard in America.

2.4. Physical Properties Characterization of Material

The X-ray diffraction analysis was performed by the Bruker-D8 instrument from Bruker in Germany. The instrument uses Cu K α as the ray source. The operating voltage was 40 kV, and the scanning speed was set at 6°/min with a scanning range of 10° to 90°.

2.5. Electrochemical Performance Test of Materials

In this paper, the constant-current charge-discharge instrument was the Xinwei battery test system (Shenzhen New Well Electronics Co., Ltd, Shenzhen, China). The charge-discharge specific capacity and cycle performance of the electrode under different current densities were studied. The charge-discharge program adopted the steps of static (15 min) → constant current discharge → static (15 min) → constant current charge → constant voltage charge. The test voltage was 0.01–3 V. The charge-discharge current value was calculated from the theoretical capacity and the mass of the active substance. The energy density, coulomb efficiency and cycle life of the electrode material could be calculated, then the stability of energy density and capacity of electrode materials in the charge and discharge processes could be judged.

The CHI660D electrochemical workstation of Shanghai Chenhua Company (Shanghai, China) was used for the cyclic voltammetry test. The scanning rate is 0.1 mV/s, and the voltage scanning range was 0.01–3.0 V.

The AC impedance test was carried out by the CHI660D electrochemical workstation. The scanning amplitude was 5 mV and the frequency range was 100 KHz–0.1 Hz.

3. Results and Discussion

3.1. The Microstructure

SEM images of Fe_2O_3 prepared by different hydrothermal temperatures are shown in Figure 1. When the temperature is 220 °C, Fe_2O_3 particles within 200–500 nm are spherical and evenly distributed. When the temperature drops to 205 °C, Fe_2O_3 particles show different morphology mainly composed of spherical and nanorod morphology. Among

them, the size of spherical particles gradually decreases, and nanorod structure appears. When the temperature decreases further to 190 °C, Fe₂O₃ particles are mostly nanorod and neatly arranges along a certain direction, and are doped with a small number of spherical particles. The size of the rod is about 100 nm calculated according to the narrowest direction. When the temperature is 175 °C, the spherical particles disappear, and the size nanorod structure is reduced to about 50 nm, which has a phenomenon of micro-agglomeration. Due to the difference in hydrothermal temperature, the growth degree of grain is different. When the temperature is low, it cannot provide enough energy to grow around the nucleation and growth processes, so the crystal can only grow in the direction of the lowest energy and form a rod structure rather than a spherical structure.

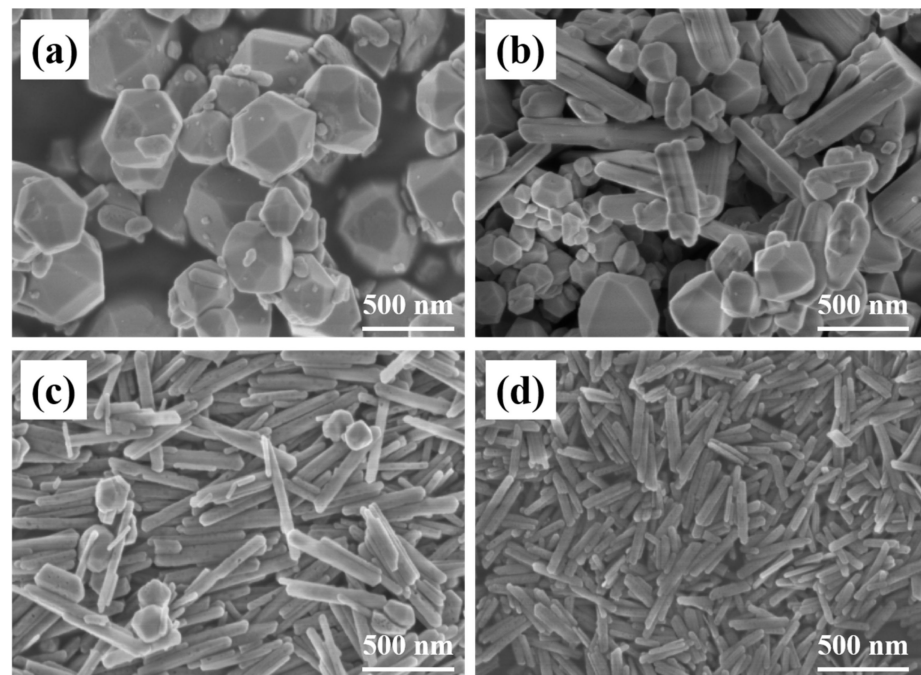


Figure 1. SEM images of Fe₂O₃ prepared at (a) 220 °C; (b) 205 °C; (c) 190 °C; (d) 175 °C.

Figure 2 is the SEM diagrams of rGO/Fe₂O₃-175 °C with different ratios of graphene, the nanorod morphology of Fe₂O₃ in rGO/Fe₂O₃-175 °C does not change significantly. From Figure 2a of 0.1rGo/Fe₂O₃-175 °C, Fe₂O₃ is slightly agglomerated on the graphene sheet, which is not conducive to buffer the volume expansion caused by Li⁺ embedding and dislodging of lithium-ion batteries during the charging and discharging process. In 0.2rGo/Fe₂O₃-175 °C, Fe₂O₃ is evenly dispersed on the surface of graphene and the size of the nanorod is reduced. It can also be seen that graphene is in small blocks and papery folds can be found. This structure can increase the specific surface area, provide more active sites and lithium storage space. However, when the ratio of graphene continues to increase, the graphene in SEM is in large chunks, and the stacking of graphene becomes more serious with the increase of graphene content [23]. It is due to the gradual thickening of graphene with the increase of GO content, that the tendency for agglomeration is enhanced, which is not beneficial for the uniform distribution of Fe₂O₃ particles, resulting in the reduction of specific surface area and the loss of lithium storage space. Therefore, 0.2rGo/Fe₂O₃-175 °C has a better structure in theory.

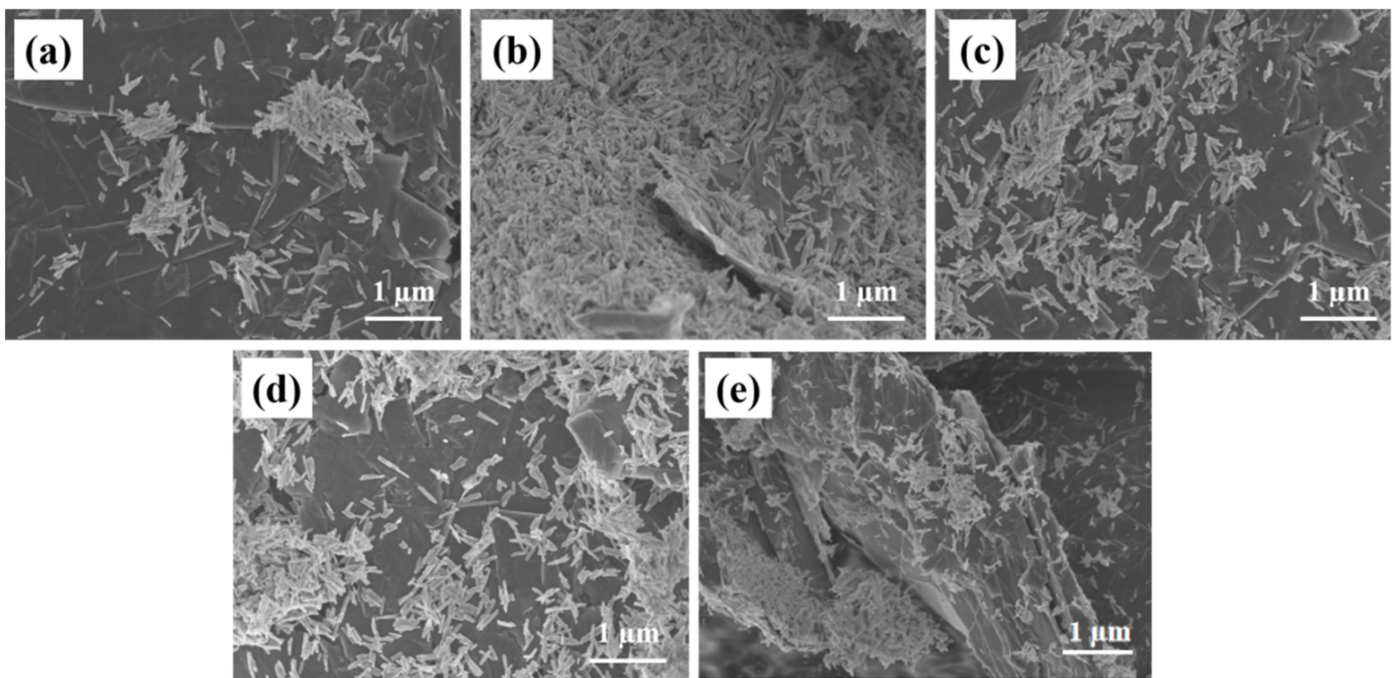


Figure 2. SEM images of rGO/Fe₂O₃-175 °C with different graphene ratios (a) 0.1; (b) 0.2; (c) 0.3; (d) 0.4; (e) 0.5.

3.2. XRD

Figure 3 shows the XRD patterns of Fe₂O₃ prepared by different hydrothermal temperatures. The sharp diffraction peak belongs to α -Fe₂O₃ (JCPDS# 89-0596) with excellent crystallinity. It can be seen that the half peak width of nanorod-shaped Fe₂O₃ is wider than that of spherical Fe₂O₃. Combined with the Scherrer formula, the grain size of nanorod-shaped Fe₂O₃ is smaller than that of spherical Fe₂O₃. It is because the energy provided for crystal growth is less with the lower temperature, leading to the reduction of the grain size of Fe₂O₃.

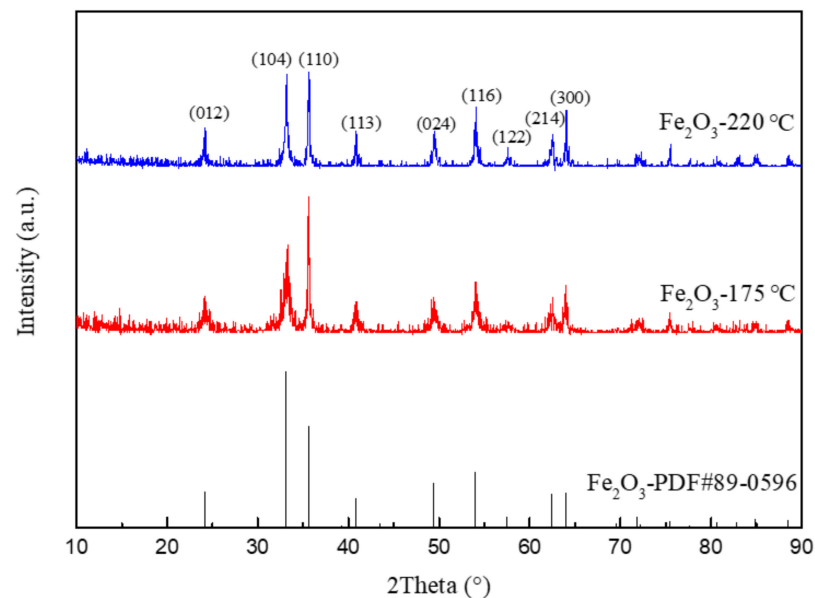


Figure 3. XRD patterns of Fe₂O₃ prepared at 220 °C and 175 °C.

Figure 4a shows the XRD pattern of GO. The diffraction peak at 10.3° is assigned to the (100) crystal plane of GO, which is the interlamellar peak of GO [24]. Figure 4b shows

the XRD patterns of rGO/Fe₂O₃-175 °C with different graphene ratios. It can be seen that the phase of the sample is composed of α -Fe₂O₃ and graphene. The characteristic peak of GO disappears completely at 10.3°, stating that the graphite oxide in the sample has been reduced, while the diffraction peak at 26.4° is attributed to the (002) crystal plane of graphite (JCPDS 08-0415), expressing that graphene has been successfully introduced into the composite sample without changing the phase structure of α -Fe₂O₃ [25]. In addition, with the increase of graphene content, the corresponding peak intensity increases.

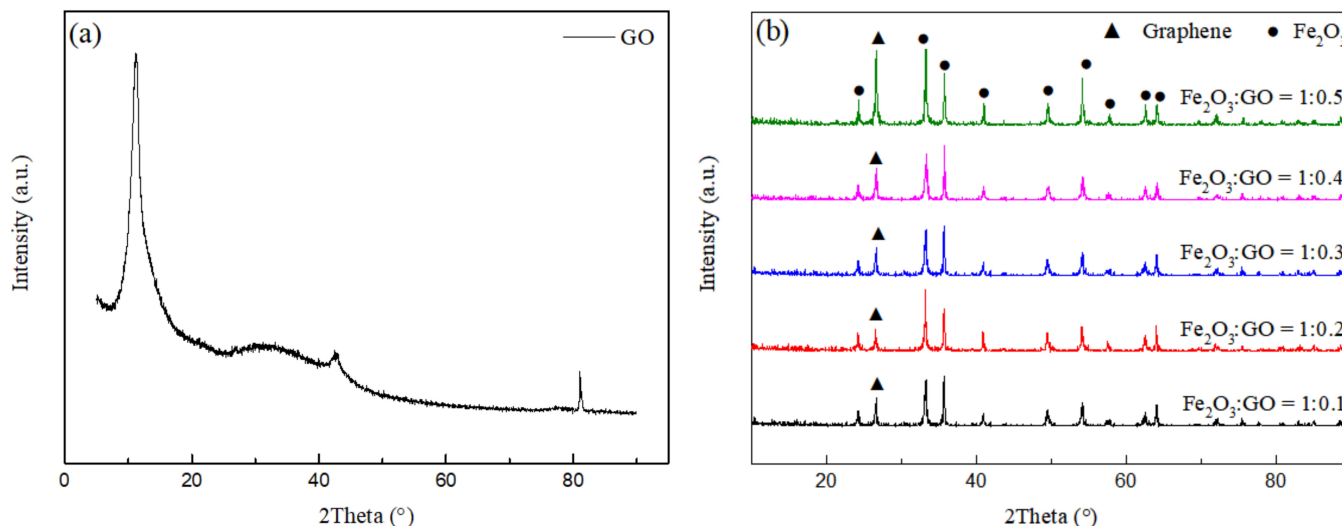


Figure 4. XRD patterns of (a) GO and (b) rGO/Fe₂O₃-175 °C with different graphene ratios.

3.3. Electrochemical Performance

As can be seen from Figure 5a, at the current density of 100 mA/g, the capacity of nanorod Fe₂O₃-175 °C for the first cycle is 1050 mAh/g, which remains stable at about 300 mAh/g after 20 cycles. Compared with spherical Fe₂O₃, the reversible capacity of nanorods Fe₂O₃ is higher in the first cycle and closer to the theoretical capacity. In addition, the capacity of nanorods Fe₂O₃ is higher after 50 cycles, in other words, it exhibits better cyclic stability. It can be concluded that the capacity decay rate of spherical Fe₂O₃-220 °C prepared at 220 °C is faster than that of nanorod Fe₂O₃-175 °C. Combined with XRD and SEM analysis, it may be due to the larger particle size of spherical Fe₂O₃-220 °C, with its own volume effect gradually causing the pulverization to fall off in the cycle process.

Compared with Fe₂O₃ in Figure 5a, it can be seen that the decay rate of rGO/Fe₂O₃-175 °C is slower than that of pure Fe₂O₃. The cycle properties of composite material are significantly improved, which is mainly due to the recombination with graphene. The existence of graphene can effectively alleviate the stress concentration caused by the volume effect of ferric oxide in the repeated charge and discharge process, and suppress the powder shedding of electrode material, to improve the cycle stability. Moreover, the cyclic capacity of 0.2rGO/Fe₂O₃-175 °C reaches 1372 mAh/g at the current density of 100 mA/g, and the cyclic decay rate is the slowest, the cyclic capacity remains at about 435 mAh/g after 50 cycles. Through SEM analysis, Fe₂O₃ is evenly distributed on the surface of graphene, and there is no stacking and agglomeration of graphene so that the high flexibility of graphene can effectively buffer the volume expansion of Fe₂O₃ nanoparticles during the cycle. With the increase of graphene content, it is easy to cause the stacking of graphene sheets and reduce the specific surface area; the loss of lithium storage space of electrode materials leads to a decrease in cycle performance.

In order to further study the rate performance of the samples, the cycling performance under different current densities is tested, as shown in Figure 5b. The discharge specific capacity of 0.2rGO/Fe₂O₃-175 °C is the highest, followed by Fe₂O₃-175 °C, and Fe₂O₃-220 °C is the lowest, which is consistent with the cyclic curve in Figure 5a. When the current density is 200 mA/g, 500 mA/g and 1000 mA/g, the discharge specific capacity

of 0.2rGO/Fe₂O₃-175 °C is kept at 905 mAh/g, 763 mAh/g and 697 mAh/g, respectively, indicating that 0.2rGO/Fe₂O₃-175 °C had excellent rate performance.

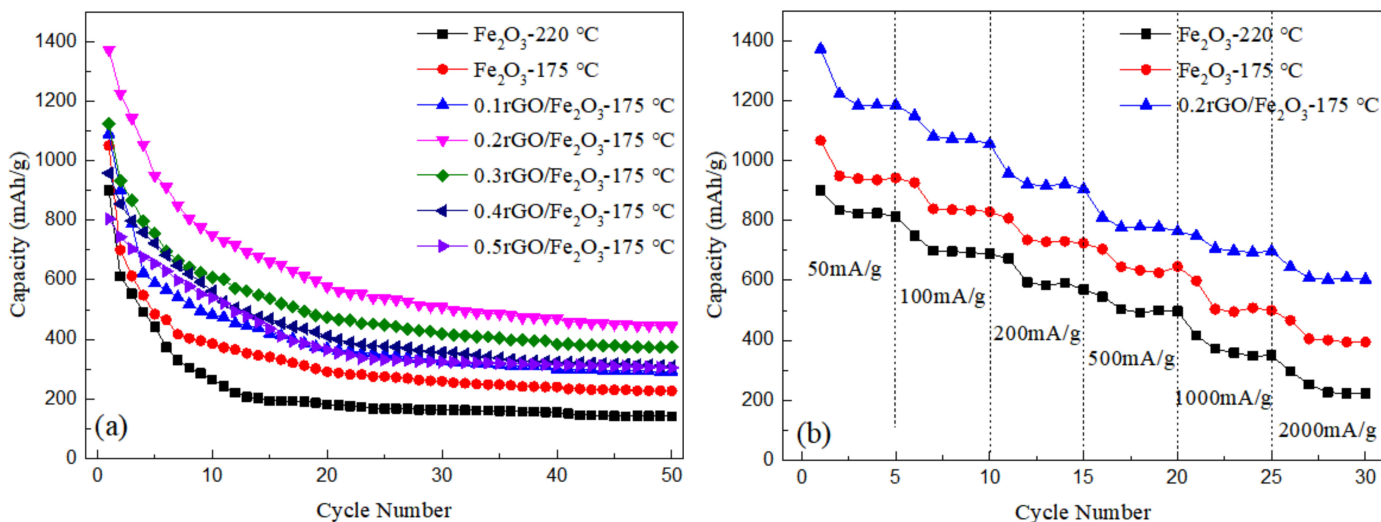


Figure 5. (a) Constant current discharge curves of Fe₂O₃ and rGO/Fe₂O₃-175 °C with different graphene ratios at a current density of 100 mA·g⁻¹; (b) Rate performance of Fe₂O₃-220 °C, Fe₂O₃-175 °C and 0.2rGO/Fe₂O₃-175 °C at different current densities.

Figure 6a,b, respectively, show the charge-discharge curves of spherical Fe₂O₃-220 °C and nanorod-like Fe₂O₃-175 °C at the current density of 100 mA/g. In the first discharge process, there is a flat discharge platform at about 0.7 V, while in the first charge curve, there is a slow platform at 1.5–2 V. The irreversible specific capacity in the first cycle is mainly due to the formation of solid electrolyte SEI film. In comparison, the first specific capacity of about 1060 mAh/g of nanorod-shaped Fe₂O₃ is larger, indicating that the small size of the nanorod-shaped structure can increase the electrochemical reaction area and improve the electrochemical capacity. Figure 6c shows the charge-discharge curve of 0.2rGO/Fe₂O₃-175 °C. Different from Fe₂O₃, two voltage platforms appear at the discharge curve in the first cycle, and one short platform and one long platform are, respectively, located around 1.6 V and 0.75 V, which is mainly related to lithium ions embedded in the Fe₂O₃ anode and the solid electrolyte phase interface (SEI film) formed by the electrolyte decomposition. In addition, the specific capacity of 0.2rGO/Fe₂O₃-175 °C for the first cycle reaches 1380 mAh/g, and the changing trend of the second cycle curve is more moderate than that of Fe₂O₃, indicating that the addition of an appropriate amount of graphene is beneficial to improving the capacity and cycle performance.

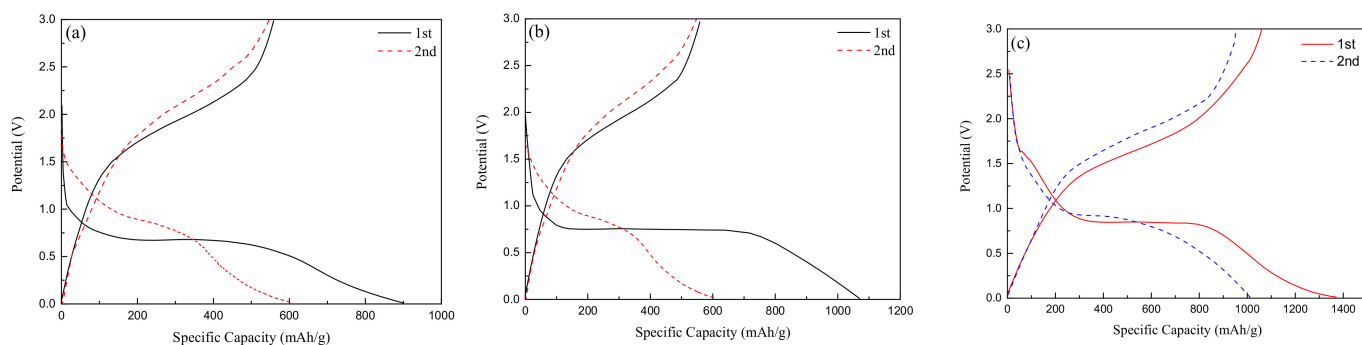


Figure 6. Charge-discharge curves of (a) Fe₂O₃-175 °C; (b) Fe₂O₃-220 °C; (c) 0.2rGO/Fe₂O₃-175 °C.

The cyclic voltammetry curve of nanorod-shaped Fe₂O₃-175 °C is shown in Figure 7a. It can be seen that in the first discharge process, the obvious cathode peak at 0.3 V corresponds to the reduction of Fe³⁺ to Fe⁰. In the first charging process, the anode peak is about

1.7 V, corresponding to the oxidation of Fe^0 into Fe^{3+} . Additionally, in the second cycle, the cathode peak moved to 0.9 V and the peak area decreased greatly, which was due to the electrolyte decomposition to form an SEI film, resulting in capacity loss [15–20]. In addition, the second and third cyclic voltammetry curves are relatively stable and show good reversibility. Figure 7b is the voltammetry curve of $0.2\text{rGO}/\text{Fe}_2\text{O}_3-175^\circ\text{C}$, which belongs to the typical voltammetry curve of metal oxide anode materials. During the first discharge process, an obvious cathode peak appears at 0.43 V, corresponding to the reaction of $\text{Li}^+ + \text{Fe}_2\text{O}_3 \rightarrow \text{Li}_x\text{Fe}_2\text{O}_3 \rightarrow \text{Fe}^0 + \text{Li}_2\text{O}$, accompanied by the decomposition of the electrolyte and the formation of an SEI film. In the first charging process, a wide anode peak appears at 1.81 V, corresponding to $\text{Fe}^0 \rightarrow \text{Fe}^{3+}$ with electrons being released [21,22]. Compared with the first discharge process, the cathode in the second discharge process moves to 0.6 V, and the peak area is also weakened. Compared with nanorod Fe_2O_3 , due to the addition of graphene, the strength of the anode peak in the curve of the $0.2\text{rGO}/\text{Fe}_2\text{O}_3-175^\circ\text{C}$ composite changes greatly, and the displacement of the cathode peak in the third cycle curve is more obvious, and the cathode peak strength is weakened.

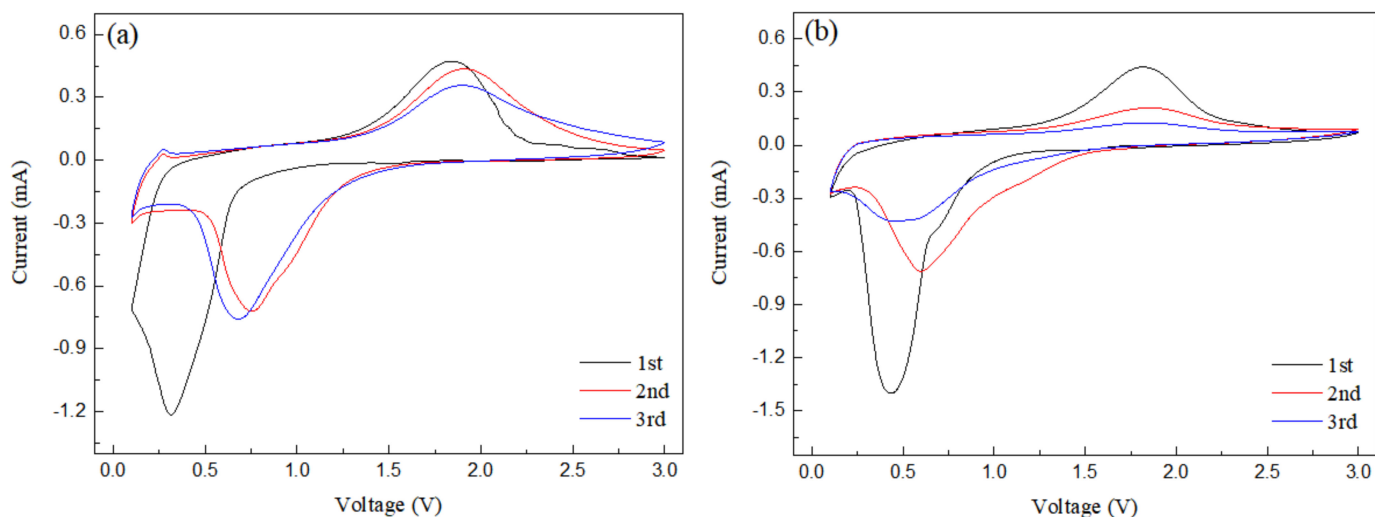


Figure 7. Cyclic voltammetry curves of (a) $\text{Fe}_2\text{O}_3-175^\circ\text{C}$; (b) $0.2\text{rGO}/\text{Fe}_2\text{O}_3-175^\circ\text{C}$.

Figure 8a shows the AC impedance diagram of Fe_2O_3 prepared at different hydrothermal temperatures and $\text{rGO}/\text{Fe}_2\text{O}_3-175^\circ\text{C}$ with different graphene ratios. EIS curves all contain a semicircle in the high frequency region and a straight line in the low frequency region. The radius of the semicircle represents the electron transfer resistance at the electrode/solution interface, that is, the charge transfer impedance at the electrode interface, which corresponds to the contact resistance of the anode material (R_{ct}). The slope of the straight line represents the mobility of lithium ions inside the electrode, namely the Warburg impedance, corresponding to the charge transfer resistance (W). The equivalent circuit fitted to the AC impedance spectrum is shown in Figure 8b. In Figure 8a, the semicircular radius of nanorod-shaped $\text{Fe}_2\text{O}_3-175^\circ\text{C}$ is smaller than that of spherical $\text{Fe}_2\text{O}_3-220^\circ\text{C}$, indicating that the former has smaller contact resistance and charge transfer resistance, which is conducive to the transmission of lithium ions. Therefore, nanorod-shaped $\text{Fe}_2\text{O}_3-175^\circ\text{C}$ has better electrochemical performance. Furthermore, it can be seen that the order of internal resistance of the composite materials is $R(1:0.2) < R(1:0.3) < R(1:0.4) < R(1:0.5) < R(1:0.1) < R(1:0)$. The R_{ct} of $0.2\text{rGO}/\text{Fe}_2\text{O}_3-175^\circ\text{C}$ anode material is $82\ \Omega$ based on the equivalent circuit, which is the minimum in $\text{rGO}/\text{Fe}_2\text{O}_3-175^\circ\text{C}$ with different graphene ratios and is basically consistent with the results of cyclic properties.

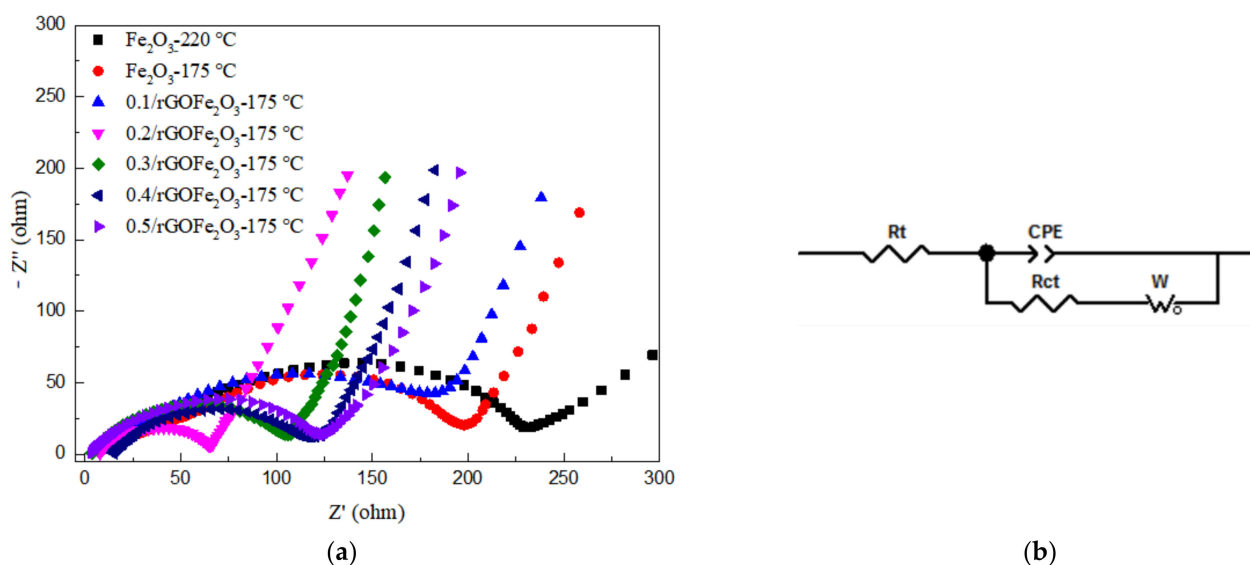


Figure 8. (a) EIS curves of Fe₂O₃-220 °C, Fe₂O₃-175 °C and rGO/Fe₂O₃-175 °C with different graphene ratios; (b) Equivalent circuit for the electrode interface. “Rt” stands for impedance; “Rct” stands for charge transfer resistance; “CPE” stands for Constant Phase Element; “W_o” stands for Warburg Element (Open).

4. Discussion

Due to the different hydrothermal synthesis temperatures of Fe₂O₃, the grain growth degree is different, leading to the grain shape and size being different. It can be seen from the XRD and SEM that the size of spherical Fe₂O₃ generated at 175 °C is much larger than that of nanorod-shaped Fe₂O₃ at 220 °C. Fe₂O₃ materials usually have a large volume expansion rate in the process of charging and discharging, which makes its capacity decay quickly and the cycle performance poor. Moreover, the small size of nanorod Fe₂O₃ as a lithium ion battery anode material can greatly buffer volume expansion in the charge and discharge process, nanoparticles have obvious advantages of electrochemical, which can effectively shorten the diffusion of lithium ions and electrons, increase the electrochemical reaction area, improve the penetration of the electrolyte, adapt to strain of Li⁺ out or embedded; so that nanorods Fe₂O₃ have better charge-discharge cycle performance than spherical Fe₂O₃.

In the preparation process of rGO/Fe₂O₃-175 °C, PVP as a surfactant can control the surface charge of nanorods α-Fe₂O₃ through the interaction between hydrophilic groups and metal oxides, and improve the dispersion of graphene [26,27]. This refinement can shorten the path of lithium ion diffusion and electron transport, and weaken the volume expansion, maintain the structural integrity and cyclic stability of the electrode. At the same time, the high softness of graphene can provide excellent intercalating space for Fe₂O₃ particles, so that Fe₂O₃ and graphene can interact more effectively, and provide free space for the volume change, which can greatly buffer the volume expansion of the composite material. In addition, Fe₂O₃ nanoparticles can also effectively prevent graphene stacking, provide a higher specific surface area, and enable more lithium ions to be embedded, thus further improving the electrochemical performance of graphene and Fe₂O₃ composites. It can be seen from the electrochemical results that the 0.2rGO/Fe₂O₃-175 °C anode material has the best cycling performance when appropriate graphene is added.

A comparison of 0.2rGO/Fe₂O₃-175 °C anode materials with other similar iron oxide and graphene composites is shown in Table 1. As can be seen from the table, researchers have used a variety of different methods in the process of composite materials synthesis, for example, the spray drying method or solvent hydrothermal method. The main morphologies of the composite materials are spherical or wafer shaped, while the morphology of 0.2rGO/Fe₂O₃-175 °C synthesized by the PVP assisted hydrothermal method in this

paper is a unique nanorod shape. In terms of electrochemical properties, it can be seen that 0.2rGO/Fe₂O₃-175 °C has a large initial discharge capacity, but the capacity after 50 cycles is lower than other compounds, which needs to be further improved.

Table 1. Comparison of synthesis methods, morphology and electrochemical properties of different iron oxide and graphene composites.

Samples	Synthetic Method	Morphology	First Charge Capacity	Capacity after 50 Cycles	Literature
graphene-encapsulated Fe ₂ O ₃	spray drying method	spheroidal	728 mAh/g	711 mAh/g	[21]
Fe ₂ O ₃ -graphene	solvent hydrothermal method	Wafer-like	1081 mAh/g	889 mAh/g	[22]
α-Fe ₂ O ₃ @graphene *	Hydrothermal self-assembly and Freeze-drying	spheroidal	1408 mAh/g	745 mAh/g	[23]
aerogel composites	PVP solvent assisted hydrothermal method	nanorod-like	1372 mAh/g	435 mAh/g	-

* Graphene coated α-Fe₂O₃.

5. Conclusions

Iron oxides materials with different morphs were prepared by different hydrothermal reaction temperatures, on this basis, rGO/Fe₂O₃-175 °C composites with different graphene ratios were synthesized and used in the cathode of lithium ion batteries. The following conclusions were drawn: The crystal phase of the hydrothermal synthesis reaction product of iron oxide is α-Fe₂O₃. With the decrease in the hydrothermal reaction temperature, the particle size of Fe₂O₃ decreased significantly, and the morphology changed from spherical Fe₂O₃ to nanorod Fe₂O₃. Nanorod-shaped Fe₂O₃ had a better electrochemical performance. rGO/Fe₂O₃-175 °C composites were prepared by PVP surfactants, which were a better fit for lithium ion insertion and release. 0.2rGO/Fe₂O₃-175 °C had the best cyclic performance and rate performance, the first cyclic discharge capacity was 1372 mAh/g under a current density of 100 mA/g. After 50 cycles, the cyclic reversible capacity remained at about 435 mAh/g, and the internal resistance was at the minimum.

Author Contributions: Conceptualization, G.Z. and B.G.; validation, G.Z.; methodology, G.Z.; formal analysis, G.Z. and H.L.; investigation, G.Z., H.L. and M.W.; resources, H.L. and M.W.; writing—original draft preparation, G.Z.; writing—review and editing, B.G.; supervision, G.T.; project administration, B.G. All authors have read and agreed to the published version of the manuscript.

Funding: This study was supported by the National Natural Science Foundation of China (51671052), the Fundamental Research Funds for the Central Universities (N182502042), the Liao Ning Revitalization Talents Program (XLYC1902105) and Shenyang Science and Technology Plan (20-203-5-39).

Institutional Review Board Statement: Not applicable.

Informed Consent Statement: Not applicable.

Data Availability Statement: The data presented in this study are available on request from the corresponding author.

Conflicts of Interest: The authors declare no conflict of interest.

References

- Cong, Y.; Ge, Y.; Zhang, T.; Wang, Q.; Shao, M.; Wang, Y. Fabrication of z-scheme Fe₂O₃-MoS₂-Cu₂O ternary nanofilm with significantly enhanced photo electro catalytic performance. *Ind. Eng. Chem. Res.* **2018**, *57*, 881–890. [[CrossRef](#)]
- Fu, Y.; Wang, X.; Wang, H.; Zhang, Y.; Yang, X.; Shu, H. An Fe₃O₄@(C-MnO₂) core-double-shell composite as a high-performance anode material for lithium ion batteries. *RSC Adv.* **2015**, *5*, 14531–14539. [[CrossRef](#)]
- Li, G.; Han, R.; Xu, X.; Ren, M. Facile synthesis of Mn-doped hollow Fe₂O₃ nanospheres coated with polypyrrole as anodes for high-performance lithium-ion batteries. *RSC Adv.* **2016**, *6*, 48199–48204. [[CrossRef](#)]
- Poizot, P.; Laruelle, S.; Grugeon, S.; Dupont, L.; Tarascon, J.M. Nano-sized transition-metal oxides as negative-electrode materials for lithium-ion batteries. *Nature* **2000**, *407*, 496–508. [[CrossRef](#)] [[PubMed](#)]
- Gu, X.; Chen, L.; Ju, Z.; Xu, H.; Yang, J.; Qian, Y. Controlled Growth of Porous α-Fe₂O₃ Branches on β-MnO₂ Nanorods for Excellent Performance in Lithium-Ion Batteries. *Adv. Funct. Mater.* **2013**, *23*, 4049–4056. [[CrossRef](#)]

6. Luo, J.; Xia, X.; Luo, Y.; Guan, C.; Liu, J.; Qi, X.; Fan, H.J. Rationally designed hierarchical TiO₂@Fe₂O₃ hollow nanostructures for improved lithium ion storage. *Adv. Energy Mater.* **2013**, *3*, 737–743. [[CrossRef](#)]
7. Yuan, S.; Zhou, Z.; Li, G. Structural evolution from mesoporous α -Fe₂O₃ to Fe₃O₄@C and γ -Fe₂O₃ nanospheres and their lithium storage performances. *CrystEngComm* **2011**, *13*, 4709–4713. [[CrossRef](#)]
8. Zhou, W.; Cheng, C.; Liu, J.; Tay, Y.Y.; Jiang, J.; Jia, X.; Zhang, J.; Gong, H.; Hng, H.H.; Yu, T. Epitaxial Growth of Branched α -Fe₂O₃/SnO₂ Nano-Hetero structures with Improved Lithium-Ion Battery Performance. *Adv. Funct. Mater.* **2011**, *21*, 2439–2445. [[CrossRef](#)]
9. Wu, M.; Ou, Y.; Lin, P. Iron oxide nanosheets and nanoparticles synthesized by a facile single-step coprecipitation method for lithium-ion batteries. *J. Electrochem. Soc.* **2011**, *158*, 231–236. [[CrossRef](#)]
10. Zhao, Y.; Feng, Z.; Xu, Z.J. Yolk-shell Fe₂O₃ circle dot C composites anchored on MWNTs with enhanced lithium and sodium storage. *Nanoscale* **2015**, *7*, 9520–9525. [[CrossRef](#)]
11. Zheng, F.; He, M.; Yang, Y.; Chen, Q. Nano electrochemical reactors of Fe₂O₃ nanoparticles embedded in shells of nitrogen-doped hollow carbon spheres as high-performance anodes for lithium-ion batteries. *Nanoscale* **2015**, *7*, 3410–3417. [[CrossRef](#)]
12. Yu, A.; Park, W.H.; Davies, A.; Higgins, C.D.; Chen, Z.; Xiao, X. Free-standing layer-by-layer hybrid thin film of graphene-MnO₂ nanotube as anode for lithium ion batteries. *J. Phys. Chem. Lett.* **2011**, *2*, 1855–1860. [[CrossRef](#)]
13. Lv, X.; Deng, J.; Wang, J.; Zhong, J.; Sun, X. Carbon-coated α -Fe₂O₃ nanostructures for efficient anode of Li-ion battery. *J. Mater. Chem. A* **2015**, *3*, 5183–5188. [[CrossRef](#)]
14. Zhao, B.; Liu, R.; Cai, X.; Jiao, Z.; Wu, M.; Ling, X. Nanorod-like Fe₂O₃/graphene composite as high-performance anode material for lithium ion batteries. *J. Appl. Electrochem.* **2014**, *44*, 53–60. [[CrossRef](#)]
15. Zhou, G.W.; Wang, J.; Gao, P.; Yang, X.; He, Y.; Liao, X.; Yang, J.; Ma, Z. Facile spray drying route for the three-dimensional graphene-encapsulated Fe₂O₃ nanoparticles for lithium ion battery anodes. *Ind. Eng. Chem. Res.* **2012**, *52*, 1197–1204. [[CrossRef](#)]
16. Zhen, Y.X.; Arbizzani, C.; Ortolani, L.; Morandi, V.; Bellani, V.; Giambastiani, G. High yield production of graphene-Fe₂O₃ nano-composites via electrochemical intercalation of nitromethane and iron chloride, and their application in lithium storage. *FlatChem* **2017**, *3*, 8–15.
17. Wang, G.X.; Shen, X.P.; Yao, J. Graphene nanosheets for enhanced lithium storage in lithium ion batteries. *Carbon* **2009**, *47*, 2049–2053. [[CrossRef](#)]
18. Yang, Y.; Feng, X.; Ivanovici, S.; Mellen, K. Fabrication of graphene-encapsulated oxide nanoparticles: Towards high-performance anode materials for lithium storage. *Angew. Chem.* **2010**, *49*, 8408–8411. [[CrossRef](#)]
19. Lian, P.; Zhu, X.; Liang, S.; Li, Z.; Yang, W.; Wang, H. High reversible capacity of SnO₂/graphene nanocomposite as an anode material for lithium-ion batteries. *Electrochim. Acta* **2011**, *56*, 4532–4539. [[CrossRef](#)]
20. Cai, D.; Li, D.; Wang, S.; Zhu, X.; Yang, W.; Zhang, S.; Wang, H. High rate capability of TiO₂/nitrogen-doped graphene nanocomposite as an anode material for lithium-ion batteries. *J. Alloys Compd.* **2016**, *561*, 54–58. [[CrossRef](#)]
21. Kan, J.; Wang, Y. Large and fast reversible Li-ion storages in Fe₂O₃-graphene sheet-on-sheet sandwich-like nanocomposites. *Sci. Rep.* **2013**, *3*, 69–74. [[CrossRef](#)]
22. Meng, J.; Fu, L.; Liu, Y.; Zheng, G.; Zheng, X.; Guan, X.; Zhang, J. Gas-liquid interfacial assembly and electrochemical properties of 3D highly dispersed α -Fe₂O₃@graphene aerogel composites with a hierarchical structure for applications in anodes of lithium ion batteries. *Electrochim. Acta* **2017**, *224*, 40–48. [[CrossRef](#)]
23. Tian, L.; Zhuang, Q.; Li, J.; Shi, Y.; Chen, J.; Lu, F.; Sun, S. Mechanism of intercalation and deintercalation of lithium ions in graphene nanosheets. *Chin. Sci. Bull.* **2011**, *56*, 3204–3206. [[CrossRef](#)]
24. Alam, S.N.; Sharma, N.; Kumar, L. Synthesis of graphene oxide (GO) by modified hummers method and its thermal reduction to obtain reduced graphene oxide (rGO). *Graphene* **2017**, *6*, 1–18. [[CrossRef](#)]
25. Liu, S.; Chen, Z.; Xie, K.; Li, Y.; Xu, J.; Zheng, C. A facile one-step hydrothermal synthesis of alpha-Fe₂O₃ nanoplates imbedded in graphene networks with high-rate lithium storage and long cycle life. *J. Mater. Chem. A* **2014**, *2*, 13942–13948. [[CrossRef](#)]
26. Yoon, S.; In, I. Role of poly(N-vinyl-2-pyrrolidone) as stabilizer for dispersion of graphene via hydrophobic interaction. *Mater. Sci.* **2009**, *46*, 1316–1321. [[CrossRef](#)]
27. Shan, C.; Yang, H.; Song, J.; Han, D.; Ivaska, A.; Niu, L. Direct electrochemistry of glucose oxidase and biosensing for glucose based on graphene. *Anal. Chem.* **2009**, *81*, 2378–2382. [[CrossRef](#)]